npj Computational Materials

www.nature.com/npjcompumats

ARTICLE OPEN

Identifying quasi-2D and 1D electrides in yttrium and scandium chlorides via geometrical identification

Biao Wan[1,2], Yangfan Lu[3,4], Zewen Xiao[3,4], Yoshinori Muraba[3], Junghwan Kim[3], Dajian Huang[2], Lailei Wu[1], Huiyang Gou[2,5], Jingwu Zhang[1], Faming Gao[5], Ho-kwang Mao[2,6] and Hideo Hosono[3,4]

Developing and understanding electron-rich electrides offers a promising opportunity for a variety of electronic and catalytic applications. Using a geometrical identification strategy, here we identify a new class of electride material, yttrium/scandium chlorides $Y(Sc)_xCl_y$ (y:$x < 2$). Anionic electrons are found in the metal octahedral framework topology. The diverse electronic dimensionality of these electrides is quantified explicitly by quasi-two-dimensional (2D) electrides for $[YCl]^+\cdot e^-$ and $[ScCl]^+\cdot e^-$ and one-dimensional (1D) electrides for $[Y_2Cl_3]^+\cdot e^-$, $[Sc_7Cl_{10}]^+\cdot e^-$, and $[Sc_5Cl_8]^{2+}\cdot 2e^-$ with divalent metal elements (Sc^{2+}: $3d^1$ and Y^{2+}: $4d^1$). The localized anionic electrons were confined within the inner-layer spaces, rather than inter-layer spaces that are observed in A_2B-type 2D electrides, e.g. Ca_2N. Moreover, when hydrogen atoms are introduced into the host structures to form YClH and Y_2Cl_3H, the generated phases transform to conventional ionic compounds but exhibited a surprising reduction of work function, arising from the increased Fermi level energy, contrary to the conventional electrides reported so far. Y_2Cl_3 was experimentally confirmed to be a semiconductor with a band gap of 1.14 eV. These results may help to promote the rational design and discovery of new electride materials for further technological applications.

npj Computational Materials (2018)4:77 ; https://doi.org/10.1038/s41524-018-0136-1

INTRODUCTION

The design and synthesis of new materials with desirable properties is essential for advancing material applications and innovations, which may influence the future of technology. One example is the recent development of electride materials that significantly promote the catalytic transformation of molecular dinitrogen into ammonia at mild reaction conditions.[1–6] Electride is a unique class of materials where the electrons are spatially confined in the vacant crystallographic sites and serve as anions to maintain charge neutrality.[7–9] The intrinsic characteristics of electrides should suggest superior electronic performances. However, the first proposed organic electrides were thermally unstable and air sensitive, constraining their technological applications.[10–12] In 2003, a room-temperature stable inorganic electride of $[Ca_{24}Al_{28}O_{64}]^{4+}(4e^-)$ was successfully synthesized by Matsuishi et al.[13] and exhibited versatile applications in many areas, including catalysts,[14,15] anode materials,[16] and an electron-injection layer in organic light-emitting diodes (OLEDs).[17] Subsequently, Ca_2N was identified experimentally to be a layer-like two-dimensional electride[18] and can be exfoliated into nanosheets.[19] The Y_2C electride was also realized experimentally and furthered our understanding of the interplay between magnetism and localized electrons.[20–23] These findings of inorganic electrides provide new possibilities for both fundamental science and applications.

Considerable experimental and theoretical investigations have been carried out to discover and produce new electrides with superior functions and capabilities. Usually, researchers arbitrarily alter the elemental combinations of typical electrides but retain their crystal symmetry to extend for the new electrides, e.g., AB-type, A_2B-type, and A_3B-type (A = alkaline or rare earth elements, B = IV, V, VI, and VII elements) electrides.[24–27] Besides, many electrides (e.g., Li,[28] Na,[29] Mg,[30] C[31], Na_2He,[32] and Sr_5P_3[33]) have been found to reveal a generalized structure under pressure.[34] Depending on the dimensionality of the anionic electrons localizations, electrides can be classified into 0D, 1D, and 2D systems,[13,20,35,36] where the anionic electrons are either isolated or bonded with each other in the cage-like, channel-like, or layer-like voids. These interesting results suggest a geometrical way to obtain the diverse 'interstitial spaces' in a lattice that can stabilize excess electrons, which can provide a vast configuration space for computational discovery.

To explore new electrides, we propose a simple strategy for identifying them by checking the local connectivity of pre-existing compositions and structures with high open frameworks. Applying high-throughput ab intio screening strategy based on the Materials Project platforms and Inorganic Crystal Structure Database (ICSD),[37–39] we focused on the reduced rare-earth yttrium and scandium chlorides (R_xCl_y, R = Y, Sc and y: $x < 2$, i.e. YCl,[40] Y_2Cl_3,[40] ScCl,[41] Sc_5Cl_8,[42] and Sc_7Cl_{10}[43]). The reduced rare-earth halides were first reported in Gd_2Cl_3.[44] Later, a series of

[1]Key Laboratory of Metastable Materials Science and Technology, College of Material Science and Engineering, Yanshan University, 066004 Qinhuangdao, China; [2]Center for High Pressure Science and Technology Advanced Research, 100094 Beijing, China; [3]Materials Research Center for Element Strategy, Tokyo Institute of Technology, 4259 Nagatsuta-cho, Midori-ku Yokohama, 226-8503 Kanagawa, Japan; [4]Laboratory for Materials and Structures, Institute of Innovative Research, Tokyo Institute of Technology, Mailbox R3-4, 4259 Nagatsuta-cho, Midori-ku, 226-8503 Yokohama, Japan; [5]Key Laboratory of Applied Chemistry, College of Environmental and Chemical Engineering, Yanshan University, 066004 Qinhuangdao, China and [6]Geophysical Laboratory, Carnegie Institution of Washington, 5251 Broad Branch Road NW, Washington, DC 20015, USA
Correspondence: Huiyang Gou (huiyang.gou@hpstar.ac.cn) or Hideo Hosono (hosono@msl.titech.ac.jp)
These authors contributed equally: Biao Wan, Yangfan Lu, Zewen Xiao, Yoshinori Muraba.

Received: 22 July 2018 Accepted: 26 November 2018
Published online: 17 December 2018

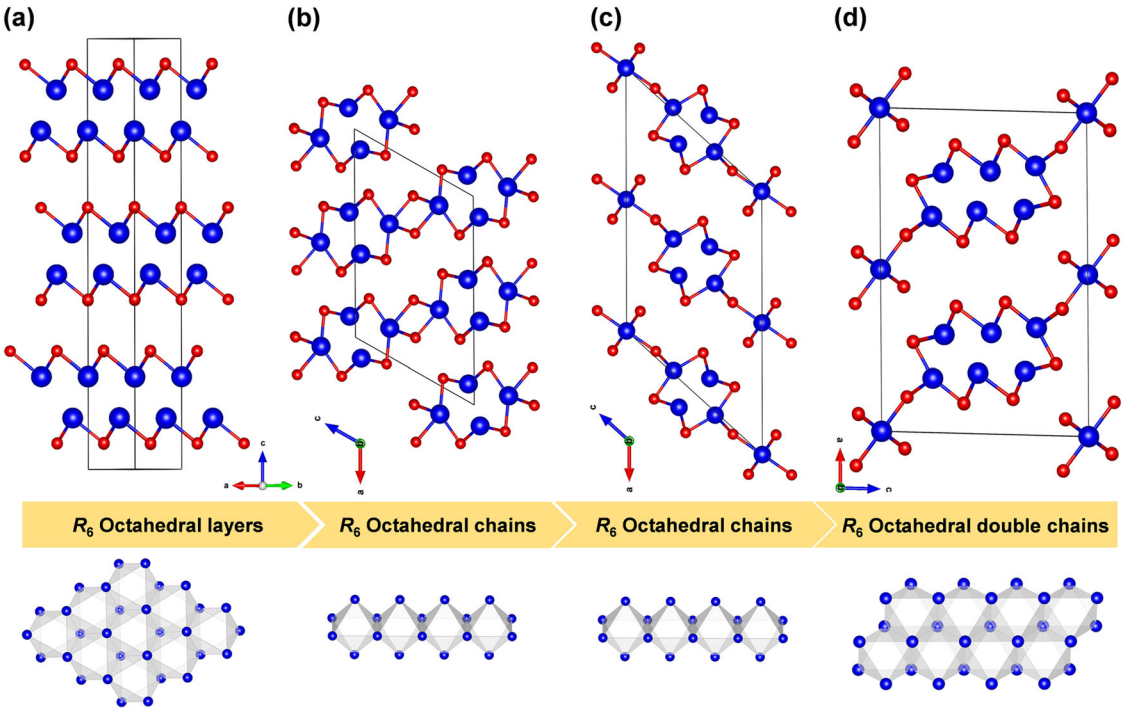

Fig. 1 Crystal structures of (**a**) YCl, (**b**) Y_2Cl_3, (**c**) Sc_5Cl_8, and (**d**) Sc_7Cl_{10}. The blue and red spheres represent the Y/Sc and Cl atoms, respectively. The edge-sharing R_6 octahedra in the host structures condensed into edge-sharing layers, chains and double chains, which are displayed at the bottom

halides were synthesized, such as, *RCh* (*R* = Sc, Y, La, Ce, Pr, Nd, Gd, Tb, and Ho, and *Ch* = Cl and Br),[40] R_2Ch_3 (*R* = Y, Gd, Tb, Er, and Lu, and *Ch* = Cl and Br),[40,44,45] R_5Ch_8 (*R* = Gd, Tb, and Sc, and *Ch* = Cl and Br),[42,46] and R_6I_7 (*R* = Er and Tb).[47] One of their characteristics is the octahedral (R_6) framework topology composed of rare-earth elements, which constitutes edge-sharing chains, double chains, or layers. Furthermore, scandium and yttrium prefer oxidation states of 2+, instead of the common oxidation state of 3+, due to the contributions of the rare earth-5*d* orbitals to the chemical bonding induced by crystal field splitting.[48,49] This unusual oxidation state gives rise to a unique chemical and physical understanding of rare-earth elements. Moreover, the various structures and compositions in *R*–*Ch* systems also provide a platform to understand the mutual coupling between excess electrons and geometrical topology and have great potential to accelerate electride discovery.

RESULTS AND DISCUSSION

Structural properties

The crystal structures of the reduced yttrium and scandium chlorides (R_xCl_y, *R* = Y, Sc, *y*: *x* < 2) are characterized by the edge-sharing R_6 octahedral layer-like (YCl and ScCl), channel-like (Y_2Cl_3 and Sc_5Cl_8), and double channel-like (Sc_7Cl_{10}) atomic voids in the host structures (Fig. 1). These voids are coated by Cl atoms and formed by variable *R*–Cl layers in the layer-like crystal structures. The metal octahedra are stretched in these structures and the *R*–*R* distances on the shared-edges are much shorter than the others. YCl crystallizes into a ZrCl-type structure (*R*-3*m*).[50,51] The Y_6 octahedral layers (Fig. 1a) were distorted and sheathed with chlorine atoms to form Cl–Y–Y–Cl close-packed layers with an interlayer distance of 3.56 Å. Two distinct Y–Y separations of 3.57 Å (shared edge) and 3.73 Å can be found in the Y_6 octahedrons that are comparable with those of 3.56 and 3.80 Å in Y_5Si_3 electride.[52] Y_2Cl_3 (Fig. 1b) is isostructural to Gd_2Ch_3 and Tb_2Ch_3 (*Ch* = Cl and Br).[44,53] The Y–Y distances in the Y_6 octahedra varied from 3.30 to 3.85 Å and the shorter Y–Y separation (3.30 Å in shared edges) suggests a stronger Y–Y interaction connected to its phase stability.[40,54] Despite being congeners of the yttrium element, the Sc–Cl system has stable stoichiometries of ScCl, Sc_5Cl_8, and Sc_7Cl_{10}.[40,42,43] ScCl crystallizes in the same structure as YCl, containing layer-like interstitial spaces formed by edge-sharing Sc_6 octahedra. Channel-like voids in Sc_5Cl_8 (Fig. 1c) and Sc_7Cl_{10} (Fig. 1d) are analogous to that of Y_2Cl_3. Due to the distortion of the Sc_6 octahedrons, the Sc–Sc bond distances change within the range of 3.26–0.52 Å for ScCl, 3.10–3.57 Å for Sc_5Cl_8, and 3.13–3.55 Å for Sc_7Cl_{10}, respectively. The shared edge in the Sc_6 octahedral chains has the minimum Sc–Sc distance, comparable to that of metal Sc (3.26 Å).

To evaluate the formation possibilities of interstitial electrons in Y–Cl and Sc–Cl compounds, we compared the configuration of interstitial voids in Y–Cl and Sc–Cl with other rare-earth-metal-containing electrides, e.g. A_2B-type compounds (anti-$CdCl_2$ structure: Y_2C, Gd_2C, Tb_2C, Dy_2C, Ho_2C, Er_2C, Sc_2C, Y_2N, La_2N, and La_2Bi; Cu_2Sb-type structure: Sc_2As, Sc_2Sb, Sc_2Bi, Y_2Sb, and Y_2Bi; others: Sc_2N, Y_2As, Y_2O, Y_2S, La_2C, La_2As, La_2Sb, La_2O, and La_2S, LaH_2, CeH_2, and YH_2)[55–57]; A_5B_3 with Mn_5Si_3-type structure (Yb_5Sb_3, Y_5Si_3)[58,59]; AB with ScBr-type structure (YBr, ScBr)[57]; $La_8Sr_2(SiO_4)_6$[35] and LaScSi.[3] Metal octahedron severing as interstitial voids can be observed in most of the host structures except Y_2O and A_2B with Cu_2Sb-type structure (Sc_2As, Sc_2Sb, Sc_2Bi, Y_2Sb, and Y_2Bi). For Cu_2Sb-type A_2B compounds, the interstitial voids can be viewed to be pseudo-octahedron (R_5X), in which the octahedron is built by five cations and one anion. To compare the interstitial volume with previously proposed electrides, the octahedral volumes of Y–X and Sc–X compounds were plotted in Fig. 2a, b. We can see that the interstitial volumes in Y–Cl (Fig. 2a) and Sc–Cl (Fig. 2b) are much higher than those of Cu_2Sb-type structure (e.g. Y_2Sb and Sc_2As), but comparable to the anti-$CdCl_2$-type Y_2N and Sc_2N. The interstitial voids in these compounds proposed here are thus believed to have large enough space to trap anionic electrons.

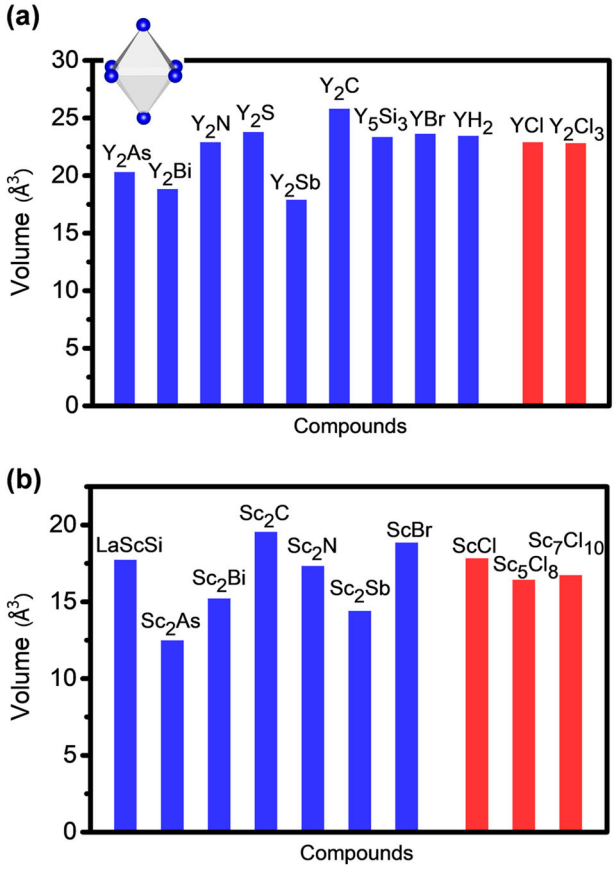

Fig. 2 Interstitial volumes of R_6 octahedron in YCl, Y_2Cl_3, ScCl, Sc_5Cl_8, and Sc_7Cl_8, comparing with other (**a**) Y and (**b**) Sc contained electrides. Interstitial volumes of R_5X octahedron in Cu_2Sb-type compounds: Sc_2As, Sc_2Sb, Sc_2Bi, Y_2Sb, and Y_2Bi were also collected

Electron localization function (ELF) analysis

To uncover the underlying electride characteristics of R_xCl_y, we first carried out analysis of the ELF of each phase.[60,61] Interestingly, as shown in Fig. 3a (YCl), Fig. 3b (Y_2Cl_3), and Fig. 3c (Sc_7Cl_{10}), two distinct ELF attractors (non-nuclear maxima in the ELF maps) off the nuclei can be observed in the center of the R_4 tetrahedra (green circle in the ELF maps, site A) and R_6 octahedra (red circle in the ELF maps, site B). The ELF attractors are more localized in the R_4 tetrahedrons but dispersed in the R_6 octahedrons. Further, the finite value of ELF between these two distinct ELF attractors suggests there is a strong interaction between them, due to their short separation (2.31 Å in YCl, 2.44 Å in Y_2Cl_3, and 2.11 Å in Sc_7Cl_{10}). However, the interspace in the R_4 tetrahedra is not large enough to hold interstitial electrons, so these ELF attractors may originate from the hybridization of the *R*-*d* orbitals, ruling out the possibility of anionic electrons in this configuration. The origin of the ELF attractors in R_4 tetrahedra is discussed in the following section. The ELF attractors observed in the metal octahedra are expected to be originated from interstitial electrons; further examinations were performed by analyzing the band structure and partial charge density.

Band structure and magnetic property

Considering the similarity in the metal frameworks of the Sc–Cl and Y–Cl systems, the band structure, and partial charge density of specified bands for YCl and Y_2Cl_3, and total and projected densities of states (TDOS and PDOS) of Y_2Cl_3 are illustrated in Fig. 4 to further uncover their electronic properties. Through analysis of the partial charges, one can unambiguously understand the bonding character of the electrons in specified bands and the band distributions of the anionic electrons. There are invariably three bands observed around the Fermi level (denoted as band 1, band 2, and band 3) in YCl (Fig. 4a) and Y_2Cl_3 (Fig. 4b). These bands are closely related to the multiple metal–metal bonding in the shared-edge of the R_6 octahedrons (Fig. 4c), which are attributed to the stretched octahedral configurations. Such multiple metal–metal bonds can usually be observed in the heavier transition metal elements, e.g., Re–Re, Mo–Mo, and W–W.[62,63] The unique divalent yttrium and scandium (Y^{2+}: $4d^15s^0$ and Sc^{2+}: $3d^14s^0$) give rise to the formation of multiple Y–Y bonds, which has not been observed in most rare earth-containing compounds (no *d* electrons in R^{3+}). The partial charge density of band 1 in Y_2Cl_3 is shown in Fig. 4d; two lobes of atomic orbitals (d_{xz}) in the Y atoms form a Y–Y π bonding within the nearest Y atoms. A similar case can be observed in the partial charge density of band 2 (Fig. 4e), where the Y-d_{yz} orbitals of the nearest Y atoms develop another Y–Y π bonding. Besides, the Y-d_{yz} orbitals (band 2) strongly overlap in the Y_4 tetrahedra forming a localized electron center, which is responsible for the presence of ELF attractors in R_4 tetrahedra. Decomposed Y-*d* orbitals also (PDOS of Y-*d* orbitals in Fig. 4c) show that the contributions from Y-d_{xz} and Y-d_{yz} are much stronger than other Y-*d* orbitals in the corresponding energy range of band 1 and band 2. The partial charge density of band 3 in YCl and Y_2Cl_3 are displayed in Fig. 4f, g, respectively. In sharp contrast with band 1 and band 2, the electrons in band 3 are loosely dispersed in the interstitial voids of the Y_6 octahedron layers (YCl) and chains (Y_2Cl_3), these electrons correspond to the ELF attractors in R_6 octahedron, which is a characteristic of electrides. The electrons in band 3 originated from the Y-5*s* orbital (Y: $4d^15s^2$ convert toY^{2+}: $4d^15s^0$, one electron in Y-5*s* orbital transferred to Cl-3*p* orbital, another is dispersed in the interstitial spaces) and two excess Y-5*s* electrons are available in their primitive cells. These electrons are confined in the interstitial spaces of the R_6 layers and chains, thus, band 3 can be described as 'an interstitial band'. Oxygen atoms have been added into the center of the R_6 octahedron in YCl and Y_2Cl_3, as shown in Fig. S1a, b, and the band 3 disappears, suggesting that it does not belong to any specific atomic orbital but an interstitial site.

To identify the contributions of interstitial electrons, the PDOS of the interstitial electrons in Y_2Cl_3 are plotted in Fig. 4c. The PDOS curves of the interstitial electrons are derived by adding a pseudoatom[20,64] with a Wigner–Seitz radius of 1.72 Å in the center of the octahedra. At the corresponding energy range of band 3, the contribution from interstitial electrons is larger than that of Y atoms. Since the size of the interstitial spaces is not large, the interstitial electron states are partially projected onto the Y-*d* orbitals (dominantly d_z^2) of the neighboring Y atoms, behaving like pseduo-σ bonds (denoted σ′). Band structure calculations reveal that YCl is ferromagnetic with a magnetic moment of 1.58 μ_B per unit cell (2YCl per formula unit). Y_2Cl_3 is a semiconductor with a calculated band gap of 0.77 eV, and no spin polarization was observed. The magnetic properties (YCl) and semiconducting behavior (Y_2Cl_3) can be understood by detailed band structure analysis. The band 1 and band 2 in Y_2Cl_3 are fully occupied by the rest of *d* electrons (Y^{2+}: $4d^15s^0$, four *d* electrons available in primitive cell Y_4Cl_6), which are attributed to the diamagnetic and semiconducting character. For YCl, analogous to Y_2Cl_3, band 1 and band 2 are contributed by two Y–Y π bonding. However, only two *d* electrons are available in the primitive cell YCl and result in the high-spin state, which leads to the ferromagnetic character with a magnetic moment of 1.58 μ_B.

The band structures and partial charge density of the interstitial bands in ScCl, Sc_5Cl_8, and Sc_7Cl_{10} are illustrated in Fig. S2a, b, c. Ferromagnetism with a magnetic moment of 1.53, 0.83, and 1.11 μ_B per unit cell is predicted for ScCl, Sc_5Cl_8, and Sc_7Cl_{10}, respectively. For Sc_7Cl_{10} (Fig. S2c), due to the double-chain configuration, four Sc–Sc π bands (two Sc-d_{yz} and two Sc-d_{xz})

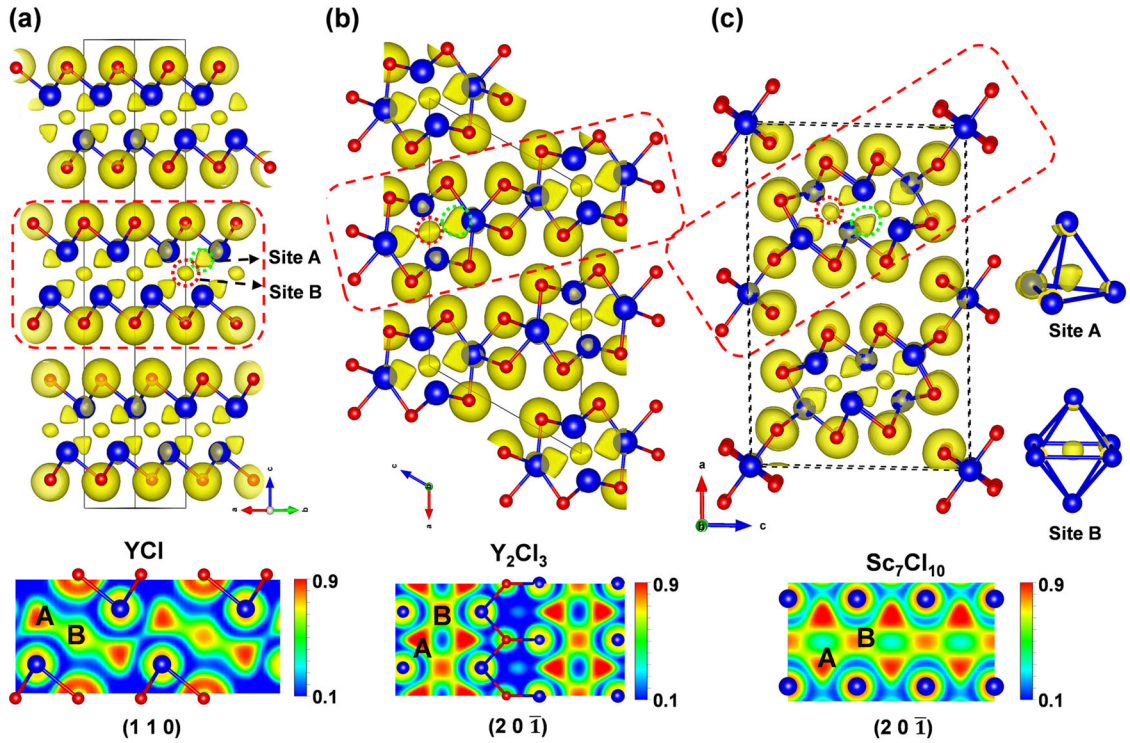

Fig. 3 The electron localization function (ELF) of (**a**) YCl, (**b**) Y_2Cl_3, and (**c**) Sc_7Cl_{10}. The isosurface value was set as 0.75, 0.75, and 0.7, respectively. The ELF attractors located at the center of the R_4 tetrahedra (site A) and the R_6 octahedra (site B) are highlighted by blue and red circles. The ELF contours in the *R*–Cl layer (guided by red dashed line in the host structures) illustrated in the (1 1 0), (2 0 −1), and (2 0 −1) planes are shown at the bottom

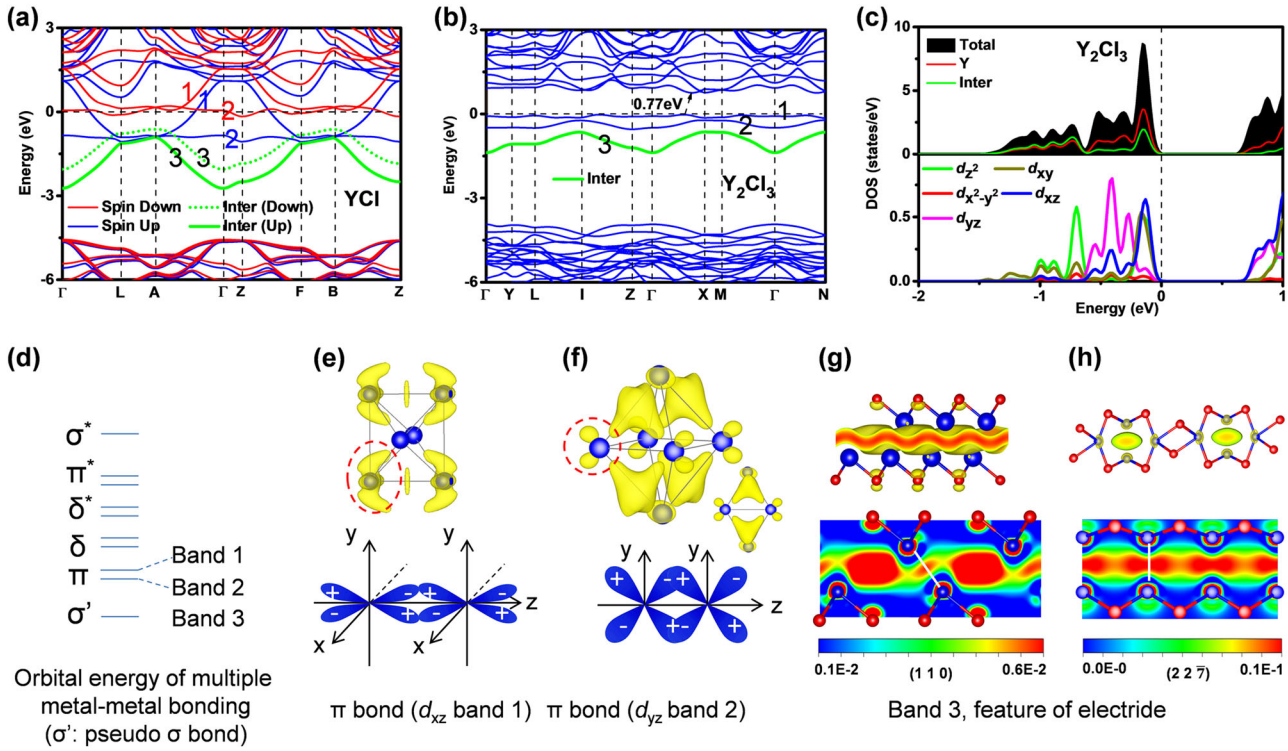

Fig. 4 Band strcrures for (**a**) YCl and (**b**) Y_2Cl_3, spin-polarized calculations are included. There are three invariable bands in YCl and Y_2Cl_3 around the Fermi level, which are denoted as band 1, band 2, and band 3. (**c**) The TDOS, PDOS curves, and Y-*d* orbitals in Y_2Cl_3, the bands where the anionic electrons confined are marked by 'inter' and green curves in band structure. (**d**) Orbital energy of multiple metal–metal bonding. Partial charge density of band 1 (**e**), band 2 (**f**) in Y_2Cl_3, the schematic diagrams for Y–Y π bonds in band 1 and band 2 are inserted. Partial charge density of band 3 in (**g**) YCl and (**h**) Y_2Cl_3, the partial charge density maps in (1 1 0) and (2 2 −7) planes are inserted, the white line between nearest Y atoms are the guide for the shared edge of nearest Y_6 octahedron

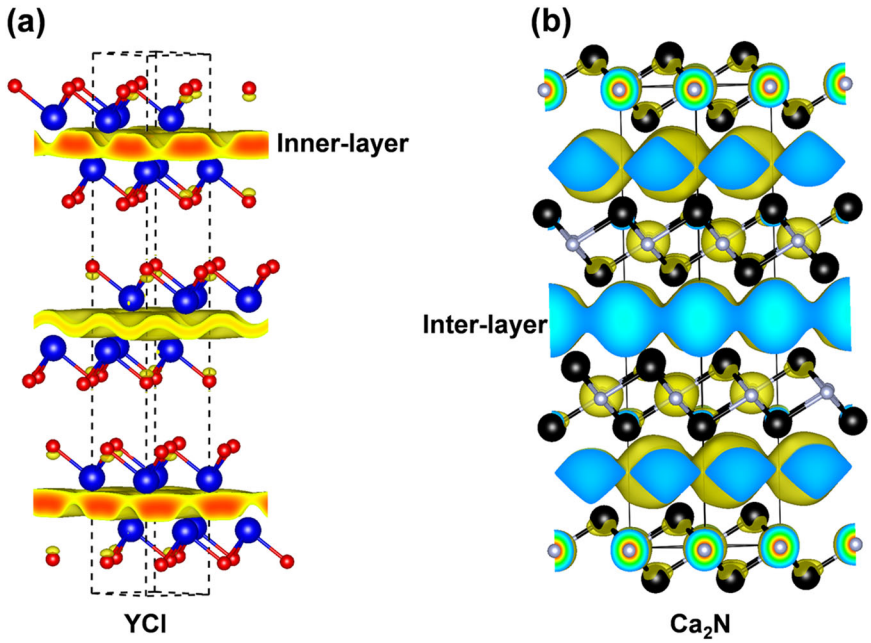

Fig. 5 Charge density of interstitial electrons in (**a**) YCl and (**b**) Ca_2N, the white and black spheres in Ca_2N represent N and Ca atoms, respectively

appear in the band structure, which leads to a magnetic moment of 1.11 μ_B per unit cell (seven Sc-3*d* electrons are available in the primitive cell). Similar to YCl and Y_2Cl_3, the partial charge (green curves in the band structure) suggests that the interstitial electrons are loosely dispersed in the R_6 metal layer or chains, which is a characteristic of electrides. The PDOS of ScCl, Sc_5Cl_8, and Sc_7Cl_{10} were also calculated through adding a pseudoatom (Wigner–Seitz radius was set as 1.65 Å in YCl, 1.61 Å in Sc_5Cl_8, and 1.61 Å in Sc_7Cl_{10}) into the interstitial sites.[20,34,64] It can be observed that, as plotted in Fig. S3a, b, c, the contributions of interstitial electrons are higher than those of Sc-*d* orbitals in the energy range where interstitial bands are distributed.

Experimental characterization has also verified the semiconducting behavior of Y_2Cl_3. As shown in Fig. S4a, b, c, a band gap of 1.14 eV for Y_2Cl_3 can be estimated (Fig. S4b). Moreover, consistent with our calculations, the magnetic measurements of the Y_2Cl_3 sample suggest its diamagnetic nature, which is significantly different from the other reduced rare-earth chlorides discussed above.

Electronic dimensionality of interstitial electrons

The distributions of the anionic electrons and the interaction between them or other atoms can significantly influence the physical and chemical properties of electrides. For YCl and ScCl, the layer-like anionic electrons show up in the inner layer of the Cl–Y–Y–Cl layers within the edge-sharing Y_6 octahedra (Fig. 5). This feature especially differs from those of typical A_2B-type 2D electrides,[24] where the interstitial spaces appear between the A_2B layers. Flat bands are observed along the L-A, Γ-Z, and F-B orientations of the interstitial bands in the band structure, which corresponds to the directions perpendicular to the Cl–Y–Y–Cl layers. The band dispersion is relatively smaller along the other directions and the anionic electrons are well confined in the 2D inner layer induced by the edge-sharing Y_6 octahedrons, giving rise to a typical 2D electride.[18,25,65] Y_2Cl_3, Sc_5Cl_8, and Sc_7Cl_{10} have similar channel voids where the anionic electrons are confined, and the interactions between the nearest anionic electrons are quite similar. The electrons confined in the metal octahedrons are weakly bonded with each other (Figs. 4h and S2b, c), and the connected anionic electrons forming 1D chains along the *b*-axis are reminiscent of previously reported 1D electrides.[33,35,59] Thus, YCl and ScCl can be regarded as quasi-2D electrides with chemical formula of $[YCl]^+\cdot e^-$ and $[ScCl]^+\cdot e^-$; Y_2Cl_3, Sc_5Cl_8, and Sc_7Cl_{10} can be regarded as quasi-1D electrides with a chemical formula of $[Y_2Cl_3]^+\cdot e^-$, $[Sc_5Cl_8]^{2+}\cdot 2e^-$, and $[Sc_7Cl_{10}]^{4+}\cdot 4e^-$ electrides.

Hydrogen absorption behavior

Typical electrides usually possess a strong hydrogen affinity caused by the effective interactions between the anionic electrons and hydrogen nuclei.[55,66] The insertion of hydrogen atoms usually occupies the positions where the anionic electrons are trapped and induces a pronounced effect on the electronic properties of electride materials. For example, hydrogen insertion makes the electrides transform to conventional ionic compounds, e.g., $C_{12}A_7$:H^-.[1,51] It was also revealed that hydrogen permeation results in the formation of $RHalH_x$ (R = Sc, Y, La, Ce, Pr, Nd, Gd, Tb, and Ho, Hal = Cl and Br, $x < \sim 1.0$);[67,68] a similar observation was also reported in Y_2Cl_3.[69] However, neutron diffraction studies suggest that hydrogen prefers to occupy the center of metal tetrahedrons instead of the R_6 octahedron.[70]

To locate the position and investigate the influence of hydrogen on the yttrium and scandium chlorides electrides, YClH and Y_2Cl_3H were constructed with hydrogen atoms located in the center of the metal tetrahedrons (crystallographic 6c site for YCl and 4i site for Y_2Cl_3). Hydrogen atoms were also added in the center of the metal octahedron, however, the imaginary phonon frequency modes confirm the loss of structural integrity with H entry into the octahedron site of YCl and Y_2Cl_3 (see Fig. S5a, b), which concurs with the experimental observation. The calculated band structures of YClH (Fig. 6a) and Y_2Cl_3H (Fig. 6b) show that the introduction of the H atom leads to Fermi level reorganization. Although the H atom has been added into the center of the metal tetrahedron, band 3, where the anionic electrons are mainly confined, vanished in both YCl and Y_2Cl_3, transforming to a conventional ionic crystal. The interstitial electrons in band 3 are found to transfer to the H 1*s* orbital caused by the strong hydrogen affinity of the interstitial electrons. Since the Y–Y π bonding (d_{yz}, band 2 in YCl, and Y_2Cl_3) formed electron maxima in the R_4 tetrahedron, the repulsion

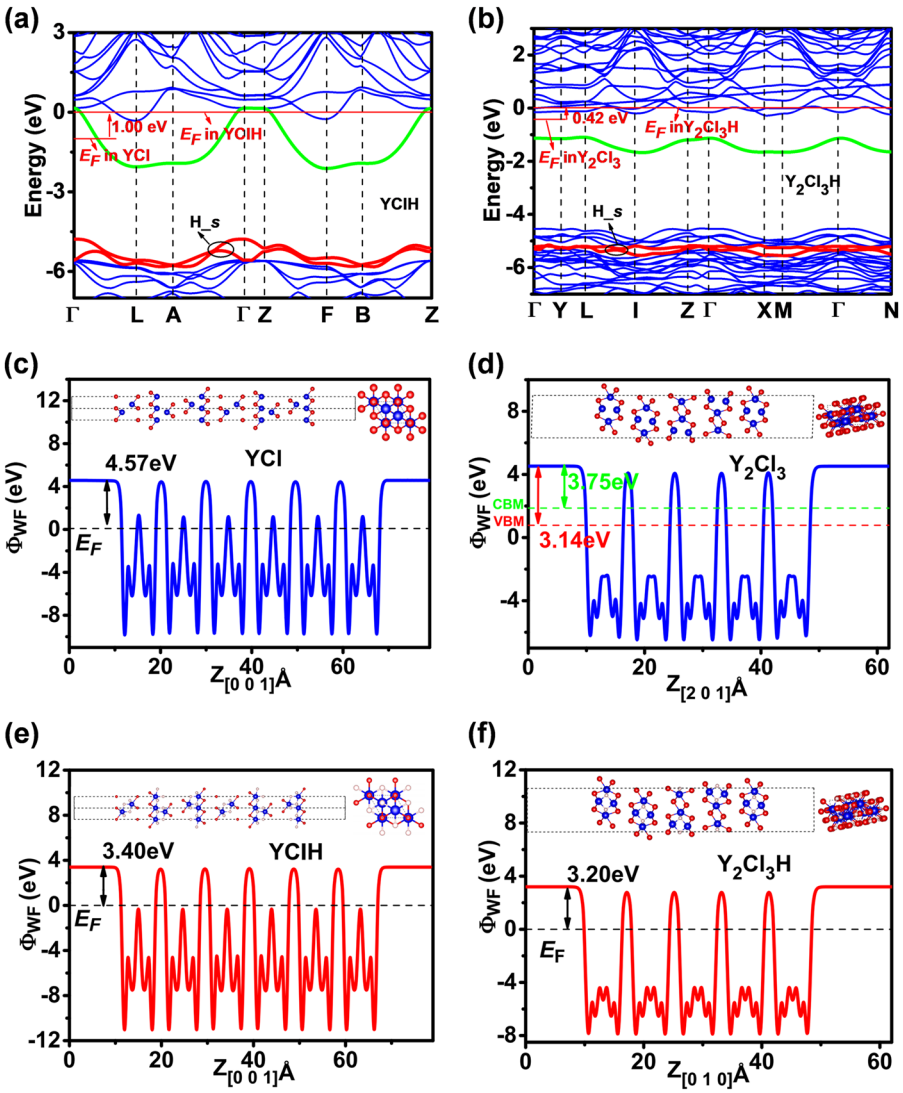

Fig. 6 Band structures and work functions for YClH (**a**, **c**, **e**) and Y_2Cl_3H (**b**, **d**, **f**). **a**, **b** Band structures. **c**, **e**, **d**, **f** Calculated work functions as a function of position (Å) along *c*-axis for YCl and YClH in the (0 0 1) surfaces, Y_2Cl_3 and Y_2Cl_3H in the (0 1 0) surfaces. The Fermi level is set as 0 eV, the Fermi level in YCl and Y_2Cl_3 is also marked by a black line in the band structures. The green curves are the band 1 in YCl and Y_2Cl_3 which remains after H absorption. The bands contributed by hydrogen atoms are marked by red curves

between H^- ($1s^2$) ions and electrons in R_4 tetrahedron significantly increases the energy of this Y–Y π bonding, which is responsible for the Fermi level reorganization. For YClH, the electrons in band 2 of YCl are transferred to another Y–Y π bonding (band 1 in YCl, d_{xz}), which leads band 1 to shift to the valence region in YClH (green curves in Fig. 6a), and no spin polarization was confirmed after hydrogen insertion. Due to the band 1 in Y_2Cl_3 being fully occupied by two Y-4*d* electrons, Y_2Cl_3H is unperturbed in Fig. 6b (green curves) and the electrons in the Y–Y π bonding of d_{yz} orbital move to the conduction band region, resulting in the significant transition from semiconductor to metal.

The intriguing locations of the H atoms drive the electrons in band 2 to transfer to other bands in a higher energy region, which significantly increases the energy at the Fermi level (1.0 and 0.42 eV higher than YCl and Y_2Cl_3, respectively, Fig. 6a, b). Such unusual variation may induce significant modification of work function (WF) (Φ_{WF}). Thus, the WFs of YCl, Y_2Cl_3, YClH, and Y_2Cl_3H were calculated. The most stable surfaces are the [0 0 1] planes for YCl and YClH, and the [2 0 1] planes for Y_2Cl_3 and Y_2Cl_3H, which are parallel to the Y–Cl layers listed in Fig. 6c–f. Consistent with the increased energy at the Fermi level, the insertion of hydrogen atoms results in a sharp decrease of WFs; 4.57 and 3.40 eV along the [0 0 1] planes for YCl (Fig. 6c) and YClH (Fig. 6e), and 3.75 eV (relative to CBM), 3.20 eV along the [0 0 1] planes for Y_2Cl_3 (Fig. 6d) and Y_2Cl_3H (Fig. 6f), respectively. Surfaces with orientations perpendicular to the Y–Cl layers were also calculated in [1 1 0] of YCl and YClH, and [0 1 0] for Y_2Cl_3 and Y_2Cl_3H. As illustrated in Fig. S6a, b, c, d, the WFs show strong anisotropic characters for these phases, similar to the typical electrides with layered structural configuration, e.g. Y_2C[20] and Ca_2N.[71] For YClH, the calculated WF of the [1 1 0] plane decreases to 2.47 eV (3.13 eV in YCl). However, the WF of the [0 1 0] planes for Y_2Cl_3H remains largely unchanged (2.81 and 2.94 eV in Y_2Cl_3 and Y_2Cl_3H). Considering the layered-like structure in the host structures, these surfaces parallel to the Y–Cl layers tend to be exposed. $YClH_{0.5}$ with H partially occupying the center of the R_4 tetrahedron was constructed to study the effect of hydrogen. As shown in Fig. S7, band 3 remains, suggesting that $YClH_{0.5}$ retains its electride nature after hydrogen absorption. The Fermi level also increased by 0.12 eV, leading to the decrease of WFs in the [0 0 1] planes. The

decreased WF after hydrogen absorption found in YCl and Y_2Cl_3 is opposite to typical electrides, which may lead to a new chemical and physical understanding of electrides.

Extending to LaCl

We also extended our study to lanthanide halide because the lanthanide elements usually possess similar chemical properties. LaCl takes the same crystal structure as YCl,[72] the band structures accompanied with an ELF and partial charge density of LaCl and LaClH (H located in the La_4 tetrahedron) are displayed in Fig. S8a, b. Similar to YCl, the partial charge density of the interstitial bands (green curves in the band structure) suggest that the interstitial electrons exist in the center of the La_6 octahedron, to form layer-like anionic electrons in the inner layer of the Cl–La–La–Cl layers, suggesting its 2D electride character. For LaClH, The variation of the Fermi level also lead to decreased WF in the [0 0 1] (from 4.51 eV in LaCl to 3.54 eV in LaClH) and [1 1 0] (from 2.81 eV in LaCl to 2.32 eV in LaClH) orientations.

Our calculations suggest that the electrides characters still remain, when hydrogen atoms occupied the center of R_4 tetrahedron partially. $LaClH_x$ ($x < 1$) was thus synthesized by the conventional solid state reaction: $LaCl_3 + La + LaH_2 > LaClH_x + ((1 - x)/2)H_2$. X-ray diffraction (XRD) pattern refinement indicates the presence of $LaClH_{0.66}$ (Fig. S9a). The amount of hydrogen incorporated in $LaClH_{0.66}$ were measured by thermal desorption spectrometry (TDS). The WF of $LaClH_{0.66}$ (Fig. S9) is determined by a cut-off energy of ultraviolet photoemission spectroscopy (UPS, hv: 21.2 eV) spectra; the obtained WF is ~3.2 eV, comparable to Y_2C (2.9 ± 0.1 eV).[20] We also calculated the WF for $LaClH_{0.5}$ through the construction of the insertion of hydrogen atoms into half of the La_4 tetrahedron. The magnitude of measured WF is between the calculated WF along the [0 0 1] and [1 1 0] planes, which are 4.01 and 2.52 eV, respectively. The large family of *R–Ch* (*R* = rare earth elements, *Ch* = Cl, Br and I) systems provides a platform to understand the mutual coupling between excess electrons and geometrical topology, which can greatly accelerate electride discovery.

In summary, we identified yttrium and scandium chlorides with various stoichiometries and compositions as a new class of quasi-2D-($[YCl]^+ \cdot e^-$ and $[ScCl]^+ \cdot e^-$) and quasi-1D-electrides ($[Y_2Cl_3]^+ \cdot e^-$, $[Sc_7Cl_{10}]^+ \cdot e^-$, and $[Sc_5Cl_8]^{2+} \cdot 2e^-$) based on geometrical identifications and high-throughput ab intio screening strategy. Anionic electrons are confined in the edge-shared R_6 octahedron. The R_6 octahedron is highly stretched, which is contributed by the multiple metal–metal bonding existing in the shared edge of the R_6 octahedron. Except Y_2Cl_3, all the other structures are ferromagnetic. Experimental measurement reveals that Y_2Cl_3 is a semiconductor with a measured band gap of 1.14 eV. These new yttrium and scandium chloride electrides have distinctive features: (i) all the structures are constituted by *R*–Cl close-packed layers, differing from those of typical A_2B-type 2D electrides, where the anionic electrons were observed in the inner *R*–Cl layer voids instead of the inter-layer spaces. (ii) The cation arrangement is characterized by the formation of edge-sharing octahedral framework topology. These R_6 octahedra constitute layer-like (YCl and ScCl), channel-like (Y_2Cl_3 and Sc_5Cl_8), and double channel-like (Sc_7Cl_{10}) interstitial spaces where the anionic electrons are confined. (iii) Hydrogen intercalations decrease the WF in YClH and Y_2Cl_3H. This is due to the unique hydrogen sites increasing the Fermi level energy. Our results provide novel insights into the basic understanding of these electrides and will stimulate continuing experimental and theoretical efforts to explore new electrides.

METHODS

The rare-earth chlorides were selected from the Materials Project platforms and ICSD,[37–39] The structural relaxations and calculations were performed using the density functional theory (DFT) as implemented in the Vienna Ab initio simulation package (VASP)[73] within the projector-augmented-wave (PAW) method.[74,75] Generalized-gradient approximation (GGA-PBE)[76] was used for the electron exchange–correlation interaction. The PAW potentials valence electrons of Y as $4s^2$, $4p^6$, $4d^1$, $5s^2$, Sc as $3p^6$, $3d^1$, $4s^2$, and Cl as $2s^2$, $3p^5$ were adopted. The plane-wave kinetic energy cutoffs were set to 600 eV, and a dense Brillouin zone sampling grid with a resolution of $2\pi \times 0.03$ Å^{-1} was chosen to ensure the enthalpy calculations converged well within 1 meV/atom. Spin-polarized calculations were considered.

To determine the WF (Φ_{WF}) of YCl and Y_2Cl_3, we constructed two slab models of [0 0 1] (24 atoms) and [1 1 0] (48 atoms) crystal planes for YCl, and [0 1 0] (90 atoms) and [2 0 1] (50 atoms) crystal planes for Y_2Cl_3, which are perpendicular or parallel to the edge-sharing metal octahedron chains (Y_2Cl_3) and layer (YCl). The vacuum was set as 25 Å for those slab models. The *k*-point grids were set as $15 \times 15 \times 1$ and $8 \times 5 \times 1$ for the [0 0 1] and [1 1 0] crystal planes of YCl, and $5 \times 4 \times 1$ and $5 \times 13 \times 1$ for the [0 1 0] and [2 0 1] crystal planes for Y_2Cl_3 using the Monkhorst–Pack method.[77] A similar set-up was applied to the YClH and Y_2Cl_3H hydrides. The Φ_{WF} value was determined using the equation: $\Phi_{WF} = E_{vac} - E_F$, where E_{vac} is the vacuum level, and E_F is the Fermi level. The crystal structure, ELF, and charge density maps were made by VESTA.[78]

The samples used in the measurements were synthesized using a conventional solid-state reaction. The elemental yttrium (turning) and YCl_3 (powder) were mixed with the ratio of Y:YCl_3 = 2:1 and sealed into an Ar-filled SUS tube. The tube was sintered twice at 750 °C for 48 h to ensure homogeneity. The obtained powders were then filtered to exclude excess yttrium. The obtained samples were black in color and sensitive to air. Powder XRD patterns were collected on a Bruker D8 advance diffractometer with CuKα radiation at room temperature. To avoid air exposure, the sample was sealed into the plastic sample holder filled with Ar gas.

The optical reflectance was measured using a UV–visible spectrophotometer (Hitachi U-4000) at room temperature. The samples were pelletized and sealed into an Ar-filled sample holder during the measurements to avoid air exposure. The magnetic properties were measured using commercial SVSM (Quantum design). $LaClH_{0.66}$ was synthesized by solid-state reaction from La metal, LaH_3 and $LaCl_3$. LaH_2 was obtained by heating metal La in a H_2 atmosphere. All starting materials and precursors were prepared in a glove box under a purified Ar Atmosphere. The mixture of starting materials was wrapped with Mo foil and placed in the sealed stainless tube; the tube was heated at 973 K for 36 h. The amount of hydrogen incorporated in $LaClH_{0.66}$ were measured by TDS (ESCO TDS-1000S/W). The WF of $LaClH_{0.66}$ was determined from a cut-off energy of ultraviolet photoemission spectroscopy (UPS, *hv*: 21.2 eV) spectra. Clean surface was prepared by cleaving the $LaClH_{0.66}$ bulk sample in the globe box that is directly connected to the UPS chamber. DC bias dependence was also checked at 5, 7, and 10 V.

DATA AVAILABILITY

The data that support the findings of this study are available from the corresponding authors, Professor Huiyang Gou of the Center for High Pressure Science and Technology Advanced Research (email: huiyang.gou@hpstar.ac.cn) and Professor Hideo Hosono of Materials Research Center for Element Strategy, Tokyo Institute of Technology (email: hosono@msl.titech.ac.jp) upon reasonable request.

ACKNOWLEDGEMENTS

This project was supported by the National Natural Science Foundation of China (NSFC) under Grants no. 51201148 and U1530402, the Thousand Youth Talents Plan. This work was also supported by MEXT Element Strategy Initiative and ACCEL of the Japan Science and Technology Agency in Japan. H.H. acknowledges MEXT KAKEHI (Grant no. 17H06153). Stay of H.G. at Tokyo Tech was supported by WRHI program. Y. F.L. was supported by the JSPS fellowship for young scientists (No. 18J00745). We also express our thanks to Prof. John Tse at the University of Saskatchewan for his instructive advice and Freyja O'Toole at HPSTAR for the English improvement. The calculations are partially supported by the High Performance Computing Center of Yanshan University.

AUTHOR CONTRIBUTIONS

H.Y.G. and H.H. designed the project. B.W., Z.W.X., D.J.H., and L.L.W. performed the calculations. Y.F.L., Y.M., and J.H.K. conducted the synthesis and characterization. B.W., Y.F.L., Z.W.X., Y.M., D.J.H., L.L.W., J.W.Z., F.M.G., H.K.M., and H.H. analyzed the data and discussed the results. B.W. and H.G. prepared the manuscript with the contributions of all authors. B.W., Y.F.L., Z.W.X., and Y.M. contributed equally to this work.

ADDITIONAL INFORMATION

Supplementary Information accompanies the paper on the *npj Computational Materials* website (https://doi.org/10.1038/s41524-018-0136-1).

Competing interests: The authors declare no competing interests.

Publisher's note: Springer Nature remains neutral with regard to jurisdictional claims in published maps and institutional affiliations.

REFERENCES

1. Kitano, M. et al. Electride support boosts nitrogen dissociation over ruthenium catalyst and shifts the bottleneck in ammonia synthesis. *Nat. Commun.* **6**, 6731 (2015).
2. Kitano, M. et al. Ammonia synthesis using a stable electride as an electron donor and reversible hydrogen store. *Nat. Chem.* **4**, 934 (2012).
3. Wu, J. et al. Tiered electron anions in multiple voids of LaScSi and their applications to ammonia synthesis. *Adv. Mater.* **29**, 1700924 (2017).
4. Kobayashi, Y., Kitano, M., Kawamura, S., Yokoyama, T. & Hosono, H. Kinetic evidence: the rate-determining step for ammonia synthesis over electride-supported Ru catalysts is no longer the nitrogen dissociation step. *Catal. Sci. Technol.* **7**, 47–50 (2017).
5. Gong, Y. et al. Ternary intermetallic LaCoSi as a catalyst for N_2 activation. *Nat. Catal.* **1**, 178–185 (2018).
6. Hara, M., Kitano, M. & Hosono, H. Ru-loaded $C_{12}A_7$:e^- electride as a catalyst for ammonia synthesis. *ACS Catal.* **7**, 2313–2324 (2017).
7. Dye, J. L. Electrides: ionic salts with electrons as the anions. *Science* **247**, 663–668 (1990).
8. Walsh, A. & Scanlon, O. D. Electron excess in alkaline earth sub- nitrides: 2D electron gas or 3D electride? *J. Mater. Chem. C* **1**, 3525–3528 (2013).
9. Dye, J. L. Electrides: early examples of quantum confinement. *Acc. Chem. Res.* **42**, 1564–1572 (2009).
10. Ellaboudy, A., Dye, J. L. & Smith, P. B. Cesium 18-crown-6 compounds. A crystalline ceside and a crystalline electride. *J. Am. Chem. Soc.* **105**, 6490–6491 (1983).
11. Landers, J. S., Dye, J. L., Stacy, A. & Sienko, M. J. Temperature-dependent electron spin interactions in lithium [2.1.1] cryptate electride powders and films. *J. Phys. Chem.* **85**, 1096–1099 (1981).
12. Singh, D. J., Krakauer, H., Haas, C. & Pickett, W. E. Theoretical determination that electrons act as anions in the electride Cs^+ (15-crown-5)$_2$·e^-. *Nature* **365**, 39 (1993).
13. Matsuishi, S. et al. High-density electron anions in a nanoporous single crystal: $[Ca_{24}Al_{28}O_6{}^{4]4+}(4e^-)$. *Science* **301**, 626–629 (2003).
14. Kanbara, S. et al. Mechanism switching of ammonia synthesis over Ru-loaded electride catalyst at metal–insulator transition. *J. Am. Chem. Soc.* **137**, 14517–14524 (2015).
15. Kuganathan, N., Hosono, H., Shluger, A. L. & Sushko, P. V. Enhanced N_2 dissociation on Ru-loaded inorganic electride. *J. Am. Chem. Soc.* **136**, 2216–2219 (2014).
16. Hu, J. et al. 2D electrides as promising anode materials for Na-ion batteries from first-principles study. *ACS Appl. Mater. Interfaces* **7**, 24016–24022 (2015).
17. Hosono, H., Kim, J., Toda, Y., Kamiya, T. & Watanabe, S. Transparent amorphous oxide semiconductors for organic electronics: application to inverted OLEDs. *PNAS* **114**, 233–238 (2017).
18. Lee, K., Kim, S. W., Toda, Y., Matsuishi, S. & Hosono, H. Dicalcium nitride as a two-dimensional electride with an anionic electron layer. *Nature* **494**, 336 (2013).
19. Druffel, D. L. et al. Experimental demonstration of an electride as a 2D material. *J. Am. Chem. Soc.* **138**, 16089–16094 (2016).
20. Zhang, X. et al. Two-dimensional transition-metal electride Y_2C. *Chem. Mater.* **26**, 6638–6643 (2014).
21. Park, J. et al. Tuning the spin-alignment of interstitial electrons in two-dimensional Y_2C electride via chemical pressure. *J. Am. Chem. Soc.* **139**, 17277–17280 (2017).
22. Park, J. et al. Strong localization of anionic electrons at interlayer for electrical and magnetic anisotropy in two-dimensional Y_2C electride. *J. Am. Chem. Soc.* **139**, 615–618 (2017).
23. Inoshita, T., Hamada, N. & Hosono, H. Ferromagnetic instability of interlayer floating electrons in the quasi-two-dimensional electride Y_2C. *Phys. Rev. B* **92**, 201109 (2015).
24. Ming, W., Yoon, M., Du, M.-H., Lee, K. & Kim, S. W. First-principles prediction of thermodynamically stable two-dimensional electrides. *J. Am. Chem. Soc.* **138**, 15336–15344 (2016).
25. Druffel, L. D., Woomer, H. A., Kuntz, L. K., Pawlik, T. J. & Warren, C. S. Electrons on the surface of 2D materials: from layered electrides to 2D electrenes. *J. Mater. Chem. C* **5**, 11196–11213 (2017).
26. Zhao, S., Li, Z. & Yang, J. Obtaining two-dimensional electron gas in free space without resorting to electron doping: an electride based design. *J. Am. Chem. Soc.* **136**, 13313–13318 (2014).
27. Park, C., Kim, S. W. & Yoon, M. First-principles prediction of new electrides with nontrivial band topology based on one-dimensional building blocks. *Phys. Rev. Lett.* **120**, 026401 (2018).
28. Miao, M., Hoffmann, R., Botana, J., Naumov, I. I. & Hemley, R. J. Quasimolecules in compressed lithium. *Angew. Chem.* **129**, 992–995 (2017).
29. Ma, Y. et al. Transparent dense sodium. *Nature* **458**, 182 (2009).
30. Li, P., Gao, G., Wang, Y. & Ma, Y. Crystal structures and exotic behavior of magnesium under pressure. *J. Phys. Chem. C.* **114**, 21745–21749 (2010).
31. Martinez-Canales, M., Pickard, C. J. & Needs, R. J. Thermodynamically stable phases of carbon at multiterapascal pressures. *Phys. Rev. Lett.* **108**, 045704 (2012).
32. Dong, X. et al. A stable compound of helium and sodium at high pressure. *Nat. Chem.* **9**, 440 (2017).
33. Wang, J. et al. Exploration of stable strontium phosphide-based electrides: theoretical structure prediction and experimental validation. *J. Am. Chem. Soc.* **139**, 15668–15680 (2017).
34. Miao, M.-S. & Hoffmann, R. High pressure electrides: a predictive chemical and physical theory. *Acc. Chem. Res.* **47**, 1311–1317 (2014).
35. Zhang, Y., Xiao, Z., Kamiya, T. & Hosono, H. Electron confinement in channel spaces for one-dimensional electride. *J. Phys. Chem. Lett.* **6**, 4966–4971 (2015).
36. Zhang, Y. et al. Electride and superconductivity behaviors in Mn_5Si_3-type intermetallics. *npj Quantum Mater.* **2**, 45 (2017).
37. Jain, A. et al. Commentary: the materials project: a materials genome approach to accelerating materials innovation. *APL Mater.* **1**, 011002 (2013).
38. Belsky, A., Hellenbrandt, M., Karen, V. L. & Luksch, P. New developments in the Inorganic Crystal Structure Database (ICSD): accessibility in support of materials research and design. *Acta Crystallogr. Sect. B* **58**, 364–369 (2002).
39. Burton, L. A., Ricci, F., Rignanese, G.-M. & Hautier, G. High-throughput identification of electrides from all known inorganic materials. Preprint at arXiv:1801.02948 (2018).
40. Mattausch, H., Hendricks, J. B., Eger, R., Corbett, J. D. & Simon, A. Reduced halides of yttrium with strong metal-metal bonding: yttrium monochloride, monobromide, sesquichloride, and sesquibromide. *Inorg. Chem.* **19**, 2128–2132 (1980).
41. Poeppelmeier, K. R. & Corbett, J. D. Metal-metal bonding in reduced scandium halides. Synthesis and crystal structure of scandium monochloride. *Inorg. Chem.* **16**, 294–297 (1977).
42. Poeppelmeier, K. R. & Corbett, J. D. Cluster condensation reactions. Synthesis and structure of pentascandium octachloride (Sc_5Cl_8). An infinite chain structure derived by cluster condensation. *J. Am. Chem. Soc.* **100**, 5039–5044 (1978).
43. Poeppelmeier, K. R. & Corbett, J. D. Metal-metal bonding in reduced scandium halides. Synthesis and characterization of heptascandium decachloride (Sc_7Cl_{10}). A novel metal-chain structure. *Inorg. Chem.* **16**, 1107–1111 (1977).
44. Lokken, D. A. & Corbett, J. D. Gadolinium sesquichloride, an unusual example of metal–metal bonding. *J. Am. Chem. Soc.* **92**, 1799–1800 (1970).
45. Lokken, D. A. & Corbett, J. D. Rare earth metal-metal halide systems. XV. Crystal structure of gadolinium sesquichloride. Phase with unique metal chains. *Inorg. Chem.* **12**, 556–559 (1973).
46. Mattausch, H. J., Simon, A. & Eger, R. Metall-rich lanthanide-bromides: Gd_5Br_8 and Tb_5Br_8. *Rev. Chim. Miner.* **17**, 516–521 (1980).
47. Karl, B., Hansjürgen, M. & Arndt, S. Neue reduzierte Halogenide der Lanthanoide mit kondensierten Clustern: Tb_6Br_7 und Er_6I_7/new reduced halides of rare earth metals with condensed clusters: Tb_6Br_7 and Er_6I_7. *Z. Nat. B* **35**, 626 (1980).
48. Mikheev, N. B., Auerman, L. N., Rumer, I. A., Kamenskaya, A. N. & Kazakevich, M. Z. The anomalous stabilisation of the oxidation state 2^+ of lanthanides and actinides. *Russ. Chem. Rev.* **61**, 990 (1992).
49. Meyer, G. & Meyer, H. J. Unusual valences in rare-earth halides. *Chem. Mater.* **4**, 1157–1168 (1992).
50. Adolphson, D. G. & Corbett, J. D. Crystal structure of zirconium monochloride. A novel phase containing metal–metal bonded sheets. *Inorg. Chem.* **15**, 1820–1823 (1976).
51. Ford, J. E., Meyer, G. & Corbett, J. D. Lithium intercalation compounds of yttrium and gadolinium monochloride: synthesis and structure. *Inorg. Chem.* **23**, 2094–2098 (1984).

52. Roger, J. et al. Mn_5Si_3-type host-interstitial boron rare-earth metal silicide compounds RE_5Si_3: crystal structures, physical properties and theoretical considerations. *J. Solid State Chem.* **179**, 2310–2328 (2006).
53. Simon, A. Condensed metal clusters. *Angew. Chem. Int. Ed. Engl.* **20**, 1–22 (1981).
54. Kremer, R. K., Mattausch, H. J., Simon, A., Steuernagel, S. & Smith, M. E. Metal–metal bonding in Y_2Cl_3—a NMR and magnetic susceptibility study. *J. Solid State Chem.* **96**, 237–242 (1992).
55. Inoshita, T., Jeong, S., Hamada, N. & Hosono, H. Exploration for two-dimensional electrides via database screening and ab initio calculation. *Phys. Rev. X* **4**, 031023 (2014).
56. Mizoguchi, H. et al. Hydride-based electride material, LnH_2 (Ln = La, Ce, or Y). *Inorg. Chem.* **55**, 8833–8838 (2016).
57. Zhang, Y., Wang, H., Wang, Y., Zhang, L. & Ma, Y. Computer-assisted inverse design of inorganic electrides. *Phys. Rev. X* **7**, 011017 (2017).
58. Lu, Y. et al. Realization of Mott-insulating electrides in dimorphic Yb_5Sb_3. *Phys. Rev. B* **98**, 125128 (2018).
59. Lu, Y. et al. Water durable electride Y_5Si_3: electronic structure and catalytic activity for ammonia synthesis. *J. Am. Chem. Soc.* **138**, 3970–3973 (2016).
60. Becke, A. D. & Edgecombe, K. E. A simple measure of electron localization in atomic and molecular systems. *J. Chem. Phys.* **92**, 5397–5403 (1990).
61. Li, Z., Yang, J., Hou, J. G. & Zhu, Q. Is mayenite without clathrated oxygen an inorganic electride? *Angew. Chem. Int Ed.* **43**, 6479–6482 (2004).
62. Chisholm, M. H. & Macintosh, A. M. Linking multiple bonds between metal atoms: clusters, dimers of "dimers", and higher ordered assemblies. *Chem. Rev.* **105**, 2949–2976 (2005).
63. Chisholm, M. H. One-dimensional polymers and mesogens incorporating multiple bonds between metal atoms. *Acc. Chem. Res.* **33**, 53–61 (2000).
64. Miao, M. & Hoffmann, R. High-pressure electrides: the chemical nature of interstitial quasiatoms. *J. Am. Chem. Soc.* **137**, 3631–3637 (2015).
65. Tsuji, Y., Dasari, P. L. V. K., Elatresh, S. F., Hoffmann, R. & Ashcroft, N. W. Structural diversity and electron confinement in Li_4N: potential for 0-D, 2-D, and 3-D electrides. *J. Am. Chem. Soc.* **138**, 14108–14120 (2016).
66. Kitano, M. et al. Essential role of hydride ion in ruthenium-based ammonia synthesis catalysts. *Chem. Sci.* **7**, 4036–4043 (2016).
67. Meyer, G., Hwu, S. J., Wijeyesekera, S. & Corbett, J. D. Synthetic study of some rare-earth-metal monohalide hydrides MXH_x and their alkali-metal intercalates. *Inorg. Chem.* **25**, 4811–4818 (1986).
68. Mattausch Hj., EgerR., Corbett, J. D. & Simon, A. Zur Darstellung von Yttriumhydridhalogeniden YXH_n (X = Cl, Br). *Z. Anorg. Allg. Chem.* **616**, 157–161 (1992).
69. Yee, K. A. & Hughbanks, T. Semilocalized bonding schemes in extended systems; orbital localization in yttrium chloride (Y_2Cl_3) and interstitial derivatives. *Inorg. Chem.* **31**, 1620–1625 (1992).
70. Wijeyesekera, S. D. & Corbett, J. D. Structure of the intermediate zirconium bromide hydride (Zr_2Br_2H) by neutron diffraction and its structural and bonding relationships to other phases. *Inorg. Chem.* **25**, 4709–4714 (1986).
71. Uijttewaal, M. A., Wijs, G. A. de. & Groot, R. A de. Low work function of the (1000) Ca_2N surface. *J. Appl. Phys.* **96**, 1751–1753 (2004).
72. Araujo, R. E. & Corbett, J. D. Lanthanum monochloride and lanthanum sesquichloride. *Inorg. Chem.* **20**, 3082–3086 (1981).
73. Kresse, G. & Furthmüller, J. Efficiency of ab-initio total energy calculations for metals and semiconductors using a plane-wave basis set. *Comput. Mater. Sci.* **6**, 15–50 (1996).
74. Blöchl, P. E. Projector augmented-wave method. *Phys. Rev. B* **50**, 17953–17979 (1994).
75. Kresse, G. & Joubert, D. From ultrasoft pseudopotentials to the projector augmented-wave method. *Phys. Rev. B* **59**, 1758–1775 (1999).
76. Perdew, J. P., Burke, K. & Ernzerhof, M. Generalized gradient approximation made simple. *Phys. Rev. Lett.* **77**, 3865–3868 (1996).
77. Pack, J. D. & Monkhorst, H. J. Special points for Brillouin-zone integrations. *Phys. Rev. B* **16**, 1748–1749 (1977).
78. Momma, K. & Izumi, F. VESTA: a three-dimensional visualization system for electronic and structural analysis. *J. Appl. Crystallogr.* **41**, 653–658 (2008).